

Analog Iterative Machine (AIM): using light to solve quadratic optimization problems with mixed variables

Kirill P. Kalinin¹, George Mourgias-Alexandris¹, Hitesh Ballani¹, Natalia G. Berloff^{2,1}, James Clegg¹, Daniel Cletheroe¹, Christos Gkantsidis^{1,*}, Istvan Haller¹, Vassily Lyutsarev¹, Francesca Parmigiani^{1,*}, Lucinda Pickup¹ and Antony Rowstron¹

¹Microsoft Research, 21 Station Road, Cambridge CB1 2FB, UK

²Department of Applied Mathematics and Theoretical Physics, University of Cambridge, Cambridge CB3 0WA, UK

*project-aim-contact@microsoft.com

Solving optimization problems is challenging for existing digital computers and even for future quantum hardware. The practical importance of diverse problems, from healthcare to financial optimization, has driven the emergence of specialised hardware over the past decade. However, their support for problems with only binary variables severely restricts the scope of practical problems that can be efficiently embedded. We build analog iterative machine (AIM), the first instance of an opto-electronic solver that natively implements a wider class of quadratic unconstrained mixed optimization (QUMO) problems and supports all-to-all connectivity of both continuous and binary variables. Beyond synthetic 7-bit problems at small-scale, AIM solves the financial transaction settlement problem entirely in analog domain with higher accuracy than quantum hardware and at room temperature. With compute-in-memory operation and spatial-division multiplexed representation of variables, AIM's design paves the path to chip-scale architecture with 100 times speed-up per unit-power over the latest GPUs for solving problems with 10,000 variables. The robustness of the AIM algorithm at such scale is further demonstrated by comparing it with commercial production solvers across multiple benchmarks, where for several problems we report new best solutions. By combining the superior QUMO abstraction, sophisticated gradient descent methods inspired by machine learning, and commodity hardware, AIM introduces a novel platform with a step change in expressiveness, performance, and scalability, for optimization in the post-Moore's law era.

Optimization is a journey, requiring identification of a task as an optimization problem, creativity in formulating it mathematically, and inventiveness in solving it. Such problems are deeply ingrained in almost every industry today, from operations

research and manufacturing, finance and engineering, to healthcare and transportation. We create an analog optimization machine that, by combining mathematical insights with algorithmic and hardware advances, could offer a crucial inflection point in the optimization journey.

Optimization workloads and machine learning applications are commonly accelerated with clusters of cloud-based digital chips such as graphical processing units (GPUs). However, the amount of required processing power is beyond traditional digital hardware that is already plateauing. Even quantum hardware cannot help with optimization at practical scales despite the promise of significant acceleration for other applications fields [1]. As a consequence, several unconventional hardware platforms for solving optimization problems have been proposed over the past decades. Prominent examples include optical parametric oscillators [2, 3, 4], memristors [5], polaritons [6, 7], coupled lasers [8], and others [9, 10, 11, 12]. Many of these approaches resort to hybrid architecture, when digital electronics is fused with the unconventional hardware to achieve scalability. Such hybrid approaches sacrifice their potential speed-up substantially. In particular, the speed-up per watt is compromised due to analog-to-digital signal conversions. For the time-multiplexed systems, where each variable is assigned a certain time slot within a single source signal, further speed-up reduction is caused by sequential processing of problem variables. These limitations motivate machines with spatially-multiplexed variables, which enable high-throughput parallel operations for spatial differentiation [13], integration [14], and solving differential equations [15]. For chip-scale platforms, the spatially-multiplexed systems promise significant speed-ups with a recent demonstration of two-variable machine [16].

Beyond the hardware limitations, most unconventional hardware optimizers, starting with pioneering Hopfield networks [17, 18], target optimization tasks described as the quadratic unconstrained binary optimization (QUBO) problem. The QUBO abstraction is a poor fit for many real-world problems [19]. In theory, an accurate solver for any NP-hard problem, such as the QUBO model, can solve all NP problems with at most polynomial overhead in number of variables, which is deemed to be negligible in algorithmic sense. In practice, the polynomial overhead may lead to significant increase in problem sizes. The overhead associated with limited hardware connectivity often results in additional substantial inflation in problem sizes [20]. Together, the mapping and limited connectivity overheads prevent the hardware solvers from tackling industrially-relevant applications at scale.

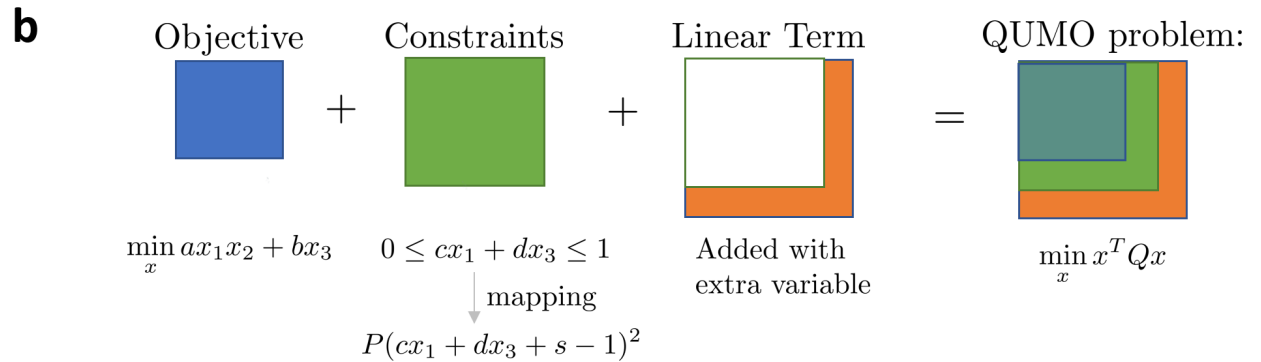
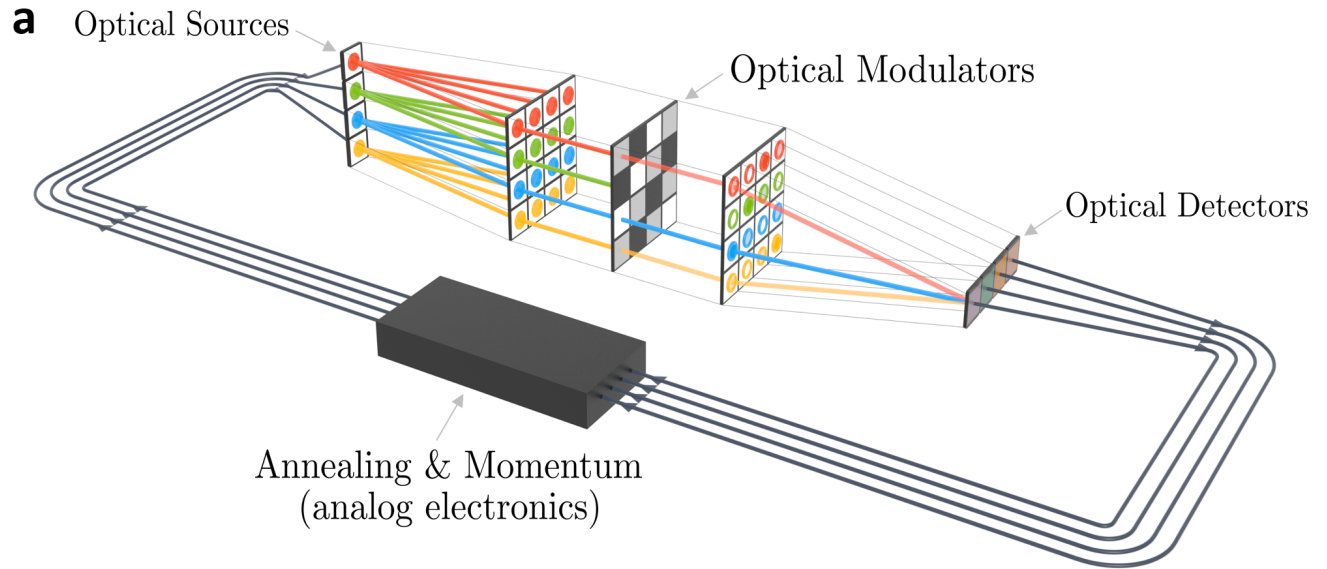
In the emerging realm of analog computation, where complex mathematical operations are performed at extremely high speed in parallel, we present the analog iterative machine (AIM) that innovates simultaneously across three dimensions — problem abstraction, algorithmic design, and analog hardware architecture — for unconventional computing paradigms.

At the abstraction level, we introduce a quadratic unconstrained mixed optimization (QUMO), which allows for both binary and continuous variables. The QUMO abstraction generalises the QUBO formulation and offers a more natural language to express quadratic optimization problems with linear inequality constraints, which results in a more efficient mapping for many applications including transaction settlement [21] and Markowitz portfolio optimization [22] problems in financial domain, crystallographic texture approximation problems in chemistry [23], and compressed sensing in healthcare [24].

At the algorithmic level, we introduce an advanced gradient descent search algorithm, inspired by well-known machine learning approaches. To overcome limitations of previous hardware approaches, whose methodology is often based on describing physical system behaviour and envisioning an improved performance of hardware thanks to natural internal processes, we focus on co-designing a highly performing algorithm and hardware from the beginning. The AIM algorithm is an iterative approach that builds on three core components: gradient of the objective function, annealing, and momentum acceleration. For the QUMO abstraction, the gradient is represented by a matrix-vector product, while annealing and momentum techniques are essential for achieving advantageous performance. All three techniques have been chosen and designed to be amenable to efficient hardware acceleration.

At the hardware level, we build the first 7-variable instance of the AIM solver based on discrete optical components. As we show schematically in Fig. 1(a), fast matrix-vector multiplication is realized using optics by representing variables as analog signal intensities, i.e., light intensities and currents, and by encoding the optimization problem as a matrix with spatial optical modulation technologies. Such design allows AIM to natively support all-to-all pairwise connectivity between the variables. The annealing and momentum techniques are well-suited for implementing in electronic domain. We report fully hardware-measured performance results for a range of QUMO problems at 7-bit precision. AIM solves all problems with an average

Figure 1: QUMO abstraction in analogue hardware. (a) The schematic of the opto-electronic system in which the iterative update rule for the gradient of the objective function, annealing, and momentum terms are implemented in analogue hardware. The problem variables are encoded in the signal intensities, namely light intensities and electrical currents, and the problem input is represented with optical modulators. (b) The optimization problems with quadratic objective and linear inequality constraints can be efficiently represented within the QUMO abstraction by introducing one additional continuous variable per constraint.



success rate over 87%, which is in agreement with the corresponding simulations. As an illustrative example of a real-world QUMO problem, that is also representative

of a broader class of industrial optimization problems, we consider the transaction settlement problem and demonstrate that AIM outperforms state-of-the-art quantum hardware [25].

Three crucial design elements of AIM pave the path to new architectures with a potential 100 times speed-up over state-of-the-art digital solvers for the same power at 10,000 variable scale. First, the data transfer between digital and analog domains is fully eliminated until convergence to a solution is achieved. Second, there is no separation between compute and memory since the variables are computed as light traverses through the optical modulation matrix. Finally, AIM leverages the inherent speed and parallelism of optics and electronics to represent each problem variable as an independent analog signal, thus eschewing the use of time-multiplexing of variables as a scaling technique. We envision that scaling to ten thousand variables is key to addressing real-world problems at scales of practical importance, and outline how the AIM architecture and technology choices open the way for such scalability at low cost.

To evaluate the AIM algorithm on problem sizes of interest, we utilize a GPU-based simulation of AIM for an extensive collection of QUBO and QUMO problems including G-Set [26], Wishart [27], Tile-3D [28], RCDP [29], and QPLIB [30] benchmarks. The QUBO problems are included to evaluate the AIM algorithm relative to the production-grade physics-inspired heuristics. Across all benchmarks, the simulated AIM demonstrates competitive and often superior solution quality, compared to state-of-the-art heuristic approaches [31], namely simulated annealing and parallel tempering, and commercial optimization package, i.e. Gurobi [32]. Moreover, the simulated AIM algorithm sets new state-of-the-art results on two QUMO and two QUBO problems from QPLIB benchmark which translate to three orders of magnitude speed-up. In doing so, the AIM algorithm demonstrates a leap forward in the capabilities of quadratic optimization algorithms.

QUMO

Optimization problems are nonlinear by their nature and, ideally, algorithms should be designed to exploit and benefit from the original problem formulation. In practice,

this approach requires a substantial expert knowledge for each class of optimization problems, resulting in their reduction to a common abstraction for which solvers exist. Given the long history of linear programming development, optimization problems are usually linearised in standard optimization packages that exploit the simplex and interior point methods. On one side, the linearisation approach allows one to treat a broad range of problems equally. On the other side, solving the problem in the form closest to the original formulation is expected to be the most efficient [33].

The QUMO abstraction represents a wide class of combinatorial nonlinear optimization problems and is formulated as the minimisation of an objective function $F(\mathbf{x})$:

$$\underset{\mathbf{x}}{\text{Minimize}} F(\mathbf{x}) = \underset{\mathbf{x}}{\text{Minimize}} -\frac{1}{2}\mathbf{x}^T Q \mathbf{x} - \mathbf{b}^T \mathbf{x} \quad (1)$$

where the vector \mathbf{x} includes binary and continuous variables, \cdot^T is the transpose operator, and the information about the optimization problem is encoded in the weight matrix Q and the constant vector \mathbf{b} . Without loss of generality, one could consider the $\{0, 1\}$ values for binary and the $[0, 1]$ interval for continuous variables. The solution to the QUMO model is the assignment of the variables \mathbf{x} that minimises the expression in [Equation 1](#). In contrast, the components of \mathbf{x} are binary variables in [Equation 1](#) for the QUBO framework.

Besides being nonlinear, most optimization problems are constrained. A problem with linear inequality constraints exemplifies the superior expressiveness of QUMO abstraction over the standard QUBO representation. As illustrated schematically in [Fig. 1\(b\)](#), only one additional continuous variable, typically referred to as slack variable, is required for mapping one inequality constraint to the QUMO abstraction with a penalty method. The resulting matrix of weights Q could also incorporate all the objective linear terms with an addition of the extra binary variable. In contrast, the QUBO model suffers from a large mapping overhead: 10 to 100 binary variables are needed to represent a single constraint with either binary or unary encoding (see Suppl. material for details). In addition, the smaller problem size implies that a better solution quality can be achieved under the same time constraints as a smaller variable space needs to be explored. We note that the QUBO model is equivalent to the well-known Ising and maximum cut models (see Suppl. Mat.).

AIM algorithm

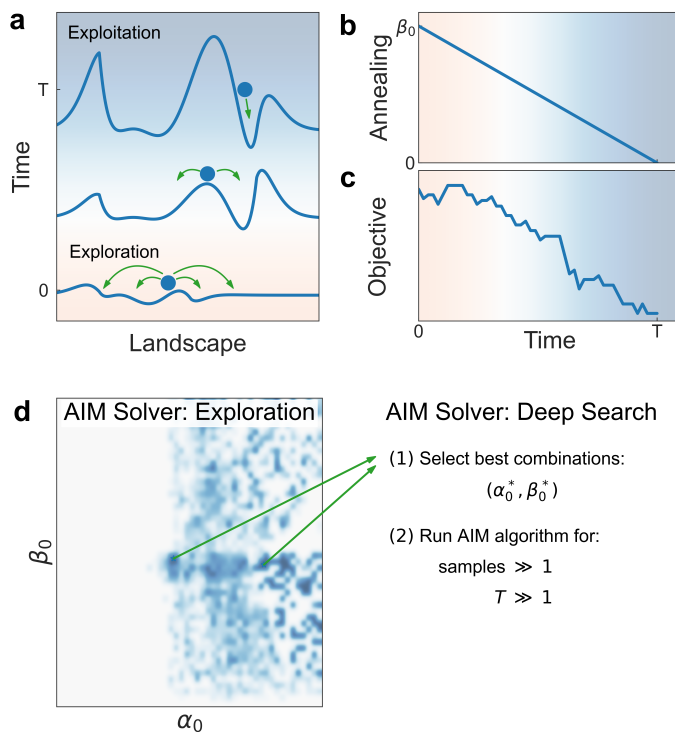
Optimization techniques may be classified into derivate-free methods and algorithms exploiting information about the gradient of the objective function, i.e., gradient-based methods. The AIM algorithm is the advanced gradient descent method, represented by the following iterative update rule:

$$\mathbf{x}_{t+1} = \mathbf{x}_t + \Delta t [-\alpha \nabla F(\mathbf{f}_{\text{nonlinear}}(\mathbf{x}_t)) - \beta(t)\mathbf{x}_t + \gamma(\mathbf{x}_t - \mathbf{x}_{t-1})], \quad (2)$$

where \mathbf{x}_t is the continuous real-valued state vector at time iteration t , Δt is the positive number known as the time step (or learning rate), ∇F is the gradient of the objective function, $\mathbf{f}_{\text{nonlinear}}(\cdot)$ is the elementwise nonlinear function that projects the variables on binary or continuous range of values, α is the objective scaling parameter, $\beta(t)$ is the annealing schedule, and γ is the momentum parameter. The term involving α on its own represents the simplest gradient descent method, known as the steepest descent, which modifies the system variables \mathbf{x}_t along the direction of the negative gradient thereby decreasing the objective. With an addition of the last term in [Equation 2](#), the steepest descent is generalised to an accelerated gradient-based approach that is known as the heavy ball method [\[34\]](#). In continuous time case, the momentum term corresponds to the dynamics of the second-order differential equation, which distinguishes the AIM algorithm from the first-order methods similar to Hopfield networks [\[17, 18\]](#). The intuition behind the momentum-based methods is simple: if one assumes that the variables \mathbf{x}_t represent coordinates of particles, then the momentum parameter is equivalent to the mass of particles moving through a viscous medium in a conservative force field [\[35\]](#). The annealing schedule $\beta(t)$ makes the system non-conservative: it characterises the system dissipation rate and controls how much the amplitude of the state \mathbf{x}_t is reduced at each time iteration t . The AIM algorithm is of a general kind and can be applied to any objective function $F(\mathbf{x})$, although in this study we will consider it for solving QUMO problems described by the [Equation 1](#).

The distinction of the AIM algorithm is the simultaneous inclusion of both momentum and annealing terms, which dramatically improve the performance of the standard steepest gradient descent method on nonconvex optimization problems. As shown schematically in [Fig. 2\(a\)](#), the annealing schedule $\beta(t)$ enhances exploration over multi-dimensional objective function space: it suppresses the contribution from the gradient of the objective function during initial time iterations, thereby flattening the objective profile. According to the above physical interpretation of

Figure 2: Analog Iterative Machine (AIM) solver. (a-c) The operational principles of the AIM algorithm are depicted schematically for a single combination of parameters. (a) The evolution of the objective landscape is shown for time iterations $t \in [0, T]$. The initially flattened landscape facilitates exploration of the multidimensional variable space and eventually returns to its original form, when exploitation occurs and the algorithm converges to the minimum of the objective. (b) The annealing term is characterized by $\beta(t)$ that decreases linearly over time, ensuring exploration and exploitation stages of the algorithm. (c) The better objective values are generally obtained towards the final time iteration T as the contribution of the objective term α increases relatively to $\beta(t)$ -term in Equation 2. (d) The two phases of the AIM solver are illustrated. During the ‘exploration phase’, the AIM algorithm is simulated for a large number of parameter combinations (α_0, β_0) with small number of time iterations and samples per each combination. During the ‘deep search’ phase, the parameter pairs (α_0^*, β_0^*) , which produce relatively better objective values during exploration phase, are selected and the AIM algorithm is simulated for a large number of time iterations and samples per each pair of parameters.



the momentum term, the massive particles accelerate their motion in long and narrow valleys, improving the convergence of the iterative approach to minima and providing mechanism for escaping from local minima. From a numerical perspective, the presence of momentum term increases the range of time step values for which the system converges [35]. In machine learning, the momentum-based approaches are known to greatly improve the speed of training, while the annealing schedule is reminiscent of slowly decaying weights and could be seen as the regularisation technique. The variations of the AIM algorithm for the Nesterov momentum and adaptive momentum methods are discussed in Supplementary materials.

The general tendency of the AIM algorithm to achieve better objective values towards the final time iteration T is ensured by relatively increasing contributions from the gradient of the objective with respect to the annealing and momentum terms. The annealing term may be time-dependent in either a linear or non-linear way although here we consider the linear schedule $\beta(t) = \beta_0(1 - t/T)$, as shown in Fig. 2(b). Hence, the annealing term decreases to zero over time and the momentum term vanishes for the equilibrium solution, which means that the AIM algorithm finds a solution corresponding to the minimum of the objective function $F(\mathbf{x})$ at time iteration T . Having such explicit stopping criteria is a lucid advantage of the AIM algorithm for an all-analog hardware implementation, as it avoids the complexity of multiple intermediate readouts that stochastic heuristic approaches suffer from [36].

We design a two-phase approach for the AIM solver to operate similar to a black-box solver that can quickly adjust the critical parameters within the given time limit, as shown in Fig. 2(d). During the ‘exploration’ phase, we evaluate the relative performance of AIM algorithm across a vast range of parameters (α_0, β_0) , where α_0 scales the α parameter by the largest eigenvalue of the weight matrix Q . A subset of ‘good’ parameters is then passed for more extensive investigation in the ‘deep search’ phase (see Methods for details).

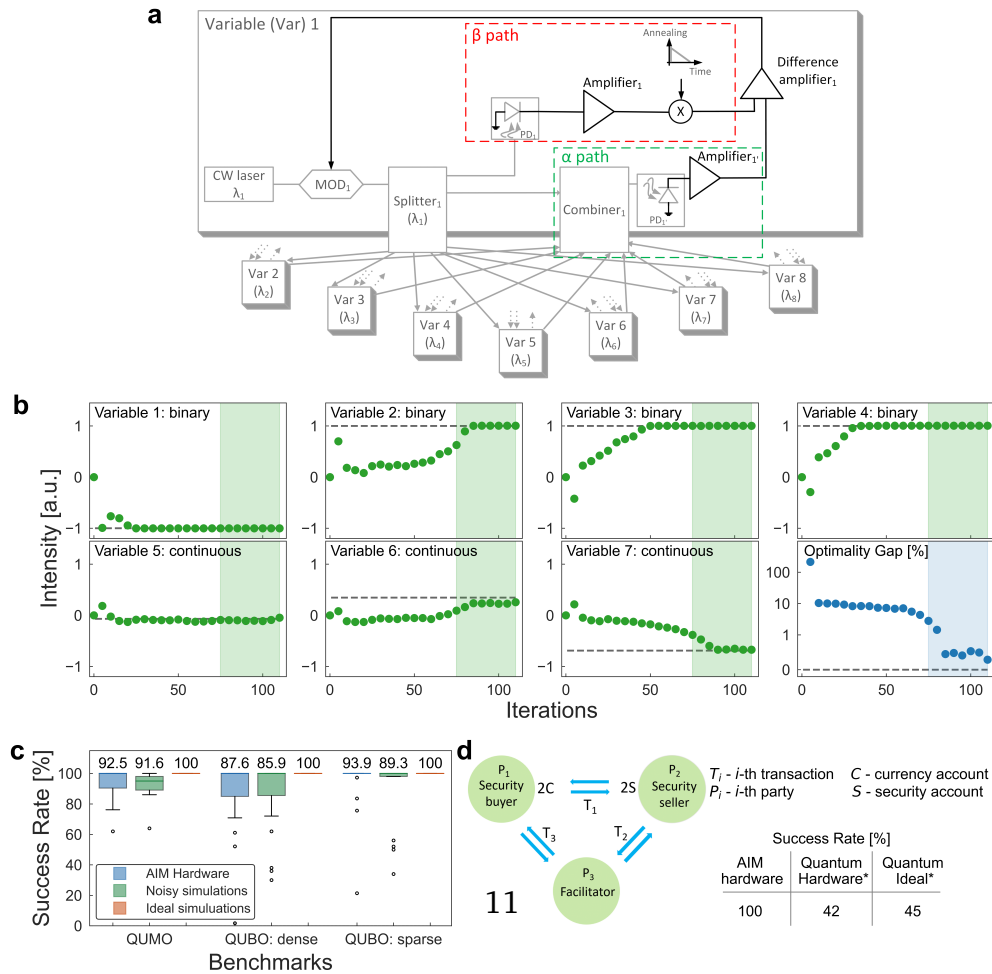
AIM Hardware Design

To surpass the speed of classical computers in solving optimization problems, the AIM algorithm is engineered to be amenable for analog hardware implementation. As a proof-of-concept, we design and build a fully analog AIM architecture with discrete opto-electronic off-the-shelf components widely available and common in telecommunication applications. We implement the most computationally expensive operation of the iterative update rule in Equation 2, namely the matrix-vector multiplication, in optical domain and the annealing characterized by $\beta(t)$ in electrical domain. The remaining momentum term could be implemented using capacitor-based time derivative circuits in the electronic domain.

Fig. 3(a) describes the operational principles of the opto-electronic hardware. In the optical domain, the values \mathbf{x}_t are encoded in the intensity of light sources. Each matrix element Q_{ij} , that represents the information about the input problem, is encoded as the transmissivity of a single cell of an optical matrix of modulators. In our specific implementation, we use multiple wavelength selective switches to emulate this modulator matrix, with each one representing a row of the matrix. As we show schematically in Fig. 3(a), the calculation of the matrix-vector product in hardware is described by three steps. During the ‘fan-out’ step, each light source within \mathbf{x}_t is split into N optical replicas, where N is the size of the problem, resulting in X_t matrix. In the ‘element-wise multiplication’ step, $Q_{ij} * (X_t)_{ij}$ is computed by shining each optical signal $(X_t)_{ij}$ onto an element of the array of modulators with transmissivity Q_{ij} . During the last ‘fan-in’ step, the intensity-modulated optical signals are summed column-wise by collecting the light onto N photodetectors. As a result, the variables have moved onto the electrical domain in the form of currents (voltages) which are proportional to the total optical power they have received and, hence, to the $Q\mathbf{x}_t$ product. In such architecture, all the scalar multiplications and additions involved in a single matrix-vector multiplication are computed in parallel in a single pass of the optical sources through the discussed setup.

To implement the annealing, we use an additional replica of the signal \mathbf{x}_t that is optically path-matched with the objective gradient arm and captured with photodetectors. The annealing $\beta(t)$ path is realized with an analog mixer, in which the signal from the path $\beta_0\mathbf{x}_t$ is multiplied with a ramp signal that has negative slope. These electrical signals are further combined with the output signals from the α

Figure 3: Hardware AIM setup and performance. (a) The setup shows the experimental implementation of the AIM algorithm based on opto-electronic components. The enhanced block represents the setup for variable 1 with the two arms corresponding to the α and β terms in Equation 2. The all-to-all connectivity is realised in hardware through the wavelength selective switches, represented as ‘combiner’ block in the scheme. (b) The signal intensities (green) and the corresponding objective optimality gap (blue) are shown as a function of time iterations for the 7-bit QUMO problem with 4 binary and 3 continuous variables. The filled light green and blue areas represent regions for steady state detection. The expected variable values and zero optimality gap are shown with grey dashed lines. (c) The success rate performance results are demonstrated for the hardware solver, its noisy simulated version, and noiseless ideal simulations of AIM algorithm across 7-bit QUMO and QUBO problems. (d) The transaction settlement problem instance involving three financial parties is mapped to the QUMO abstraction and solved in hardware with a success rate of 100%.



path and supplied back to the corresponding modulated sources, completing one iteration of the AIM algorithm.

On each iteration, the nonlinearity is introduced into the system through the combination of optical sources with the square-law detection scheme and the saturation of analog electronics. By calibrating the gain of each amplifier prior to the modulator, we select a specific region of the transfer function to realise either binary or continuous variables. The closed loop system allows signals to remain in analog domain for hundreds of iterations until the annealing term vanishes. At this point, the signal amplitudes are read out digitally and the optimised objective value can be computed for the original problem.

Opposed to the variable encoding in phase domain, encoding variables as light intensities can bring a notable scaling advantage, as the precision requirements for calibrating variable paths are proportional to the system GHz bandwidth and not the bandwidth of the optical sources, which can reach 10^5 GHz. At the same time, the intensity encoding constrains one to operate with nonnegative matrix weights. For a general matrix-vector product, one can apply offsetting and scaling procedures to represent operations with arbitrary matrix weights in analog domain [37, 38].

Such opto-electronic architecture offers a simple blueprint of analog hardware for solving hard optimization problems with binary and continuous variables.

AIM hardware performance and cross-validation

We conduct a comprehensive evaluation of the opto-electronic AIM solver on a diverse set of QUMO and QUBO problems. The AIM can solve optimization problems with binary and continuous variables, with arbitrary connectivity, dense or sparse, and with 7 bits accuracy for the problem input weights. We vary the parameters (α_0, β_0) within their accessible range in hardware to identify the optimal parameter combination for sampling. For a representative QUMO instance, we present the time evolution of variables and optimality gap in Fig. 3(b). The optimality gap is defined in a conventional way as the ratio of the difference between the best objective and the found objective to the best objective. The steady states are detected within the

shaded regions. For the measured binary and continuous variable values, we obtain a high-quality solution to the QUMO problem, with a final optimality gap of 0.29%, in an entirely analog manner without any digital pre- and post-processing.

We cross-validate the simulated AIM solver and its discrete opto-electronic implementation on 50 instances of the QUMO and QUBO models. Given the historical emphasis on the QUBO model, we consider 40 QUBO instances with 8 variables, representing problem classes that are known to be computationally challenging at scale. These instances are divided equally between two graph topologies, namely dense fully-connected and sparse three-regular graphs. In both cases, the matrix weight elements are drawn from the Gaussian distribution and their bit precision is reduced to 7 bits, resulting in instances belonging to the Sherrington-Kirkpatrick [39] and weighted maximum cut problems. Given the novel nature of the QUMO abstraction, there is a lack of research on methods for generating challenging small size instances with a mixture of binary and continuous variables. We develop a technique for planting random continuous minimizer values in the global solution and generate 10 QUMO instances with 7 variables. To make these instances more challenging to solve and obscure the planted solutions, hundreds of random perturbations are applied to their matrix weights.

In Fig. 3(c), the success rates of the opto-electronic solver are presented for the QUBO and QUMO instances. The success rate, a widely used metric for evaluating the performance of heuristic solvers, is defined as the probability of finding the global objective value for a given set of parameters. The hardware solver targets exact objective values for the QUBO instances while the relative and absolute tolerances are set to 99.5% for QUMO instances to account for hardware imperfections. For all benchmarks, the opto-electronic AIM achieves high average success rates over 87.6% with a median success rate of 100%. This performance is in agreement with that of the simulated noisy AIM algorithm, and is closely aligned with the performance of the simulated noiseless AIM algorithm.

The opto-electronic AIM demonstrates exceptional performance on challenging synthetic QUMO and QUBO instances at small scale. While the hardware solver finds global objectives for all instances, there are several outliers for which the success rates are lower, with values of about 62%, 1.7%, and 21.4% across the QUMO, QUBO (dense), and QUBO (sparse) benchmarks. Such outliers may be attributed to the

inaccessible range of optimal parameter values or to the particular nonlinear function implemented in hardware.

Solving Transaction Settlement Problem with AIM hardware

As a demonstration of the QUMO abstraction importance, we further consider an industrially important problem from financial domain, namely the transaction settlement problem, and solve it with AIM hardware. This problem arises in the context of financial transactions when one needs to ensure that the parties involved in the transaction are able to receive the funds or assets that they are entitled to in a timely and efficient manner, as shown schematically in Fig. 3(d). If one party fails to meet their obligations, the securities settlement system may not be able to settle all transactions, which can cause a chain reaction of many unsettled transactions. Consequently, transaction settlement is the NP-hard optimization problem of finding the optimal set of transactions to settle [40].

Various approaches have been proposed for solving the transaction settlement problem, one of which formulates it as a linear binary optimization problem with linear inequality constraints [21]. In turn, the transaction settlement problem can be further mapped to the QUMO abstraction since the inequality constraints can be efficiently incorporated into the objective function by introducing continuous slack variables.

Here we consider a problem instance that is derived from real settlement data [21]. In order to fit the current hardware requirements, we reduce the original small-scale problem with 9 variables to 6 variables, i.e., 3 binary and 3 continuous. We observe the high success rates of 99% and 100% for both, the hardware AIM and its simulated version in Fig. 3. For comparison, we highlight the quantum hardware and simulated quantum hardware performance for the same problem with a success rate of 45% and 42%, respectively [21].

Simulated AIM Solver Performance at scale

Here we validate the algorithmic performance of the AIM solver that is implemented on the GPU. We consider a comprehensive set of benchmarks, one of which is the quadratic programming library (QPLIB). The QPLIB benchmark is a collection of challenging synthetic and real-world problems, gathered over a year-long open call from mathematical and numerical analysis communities [30, 41]. For evaluating the AIM solver on QUMO problems, we focus on a subset of QPLIB benchmark, namely the non-convex problems with linear inequality constraints. These problems have up to several thousand variables, while the number of constraints reaches ten thousand. These constraints lead up to ten thousand additional continuous variables for problems formulated within the QUMO abstraction. We consider unconstrained and equality-constrained binary problems within QPLIB. In addition, we use the well-studied G-Set benchmark with synthetically generated problems up to 20000 variables [26], Tile3D and Wishart instances from a recently introduced CHOOK generator [42], as well as a set of manufacturing problems, i.e., RCDP.

For QUMO problems, we compare the AIM approach against the commercial Gurobi solver, that outperforms such optimization packages as Octeract, Baron, and Scip [43]. For QUBO benchmarks, in addition to Gurobi, we consider two heuristic approaches, namely simulated annealing and parallel tempering, that are known for a consistently better or similar performance over other physics-inspired methods [44, 45, 46]. Both heuristic approaches benefit from highly-optimised implementations in Azure quantum inspired optimization service and work as black-box solvers for a given time limit [31].

We design the AIM approach to resemble a black-box solver operation with the main sensitive parameters (α_0, β_0) dynamically adjusted for a given time limit for each problem, while small variations of the momentum parameter values are explicitly mentioned within and between benchmarks (see Suppl. Mat.). For a representative performance comparison across such a disparate set of benchmarks,

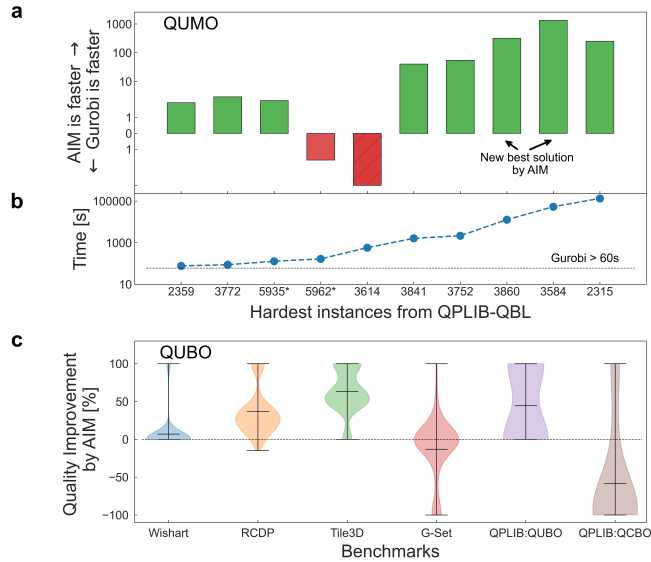
we consider the quality of solution improvement metric:

$$\text{Objective Improvement} = \begin{cases} 100\% \cdot \frac{F_{\text{AIM}} - F_{\text{Best_rest}}}{F_{\text{Best_known}} - F_{\text{Best_rest}}}, & \text{if AIM is better than all competing methods} \\ 0\%, & \text{if AIM is equal to the best competing method} \\ -100\% \cdot \frac{F_{\text{Best_rest}} - F_{\text{AIM}}}{F_{\text{Best_known}} - F_{\text{AIM}}}, & \text{if AIM is worse than the best competing method} \end{cases} \quad (3)$$

where $F_{\text{Best_known}}$ represents the best known minimum of the objective function for the problem and the AIM algorithm is compared against the best solution found by competing solvers: Gurobi, parallel tempering, or simulated annealing. Since all solvers are given the same computational resources equivalent to about 100 seconds of the AIM solver, the solution improvement metric serves as a good indicator of their relative performance in terms of finding better objective function values (see Methods).

For the QUMO benchmark, we report the AIM speed-up against the Gurobi solver on the hardest quadratic binary problems with linear inequality constraints within QPLIB (QPLIB:QBL). Since Gurobi attempts not only to find the optimal solution, but also to prove the global optimality of the solution, we consider the Gurobi time when it first finds the best objective value, which can be compared with the time of the AIM solver, that provides no global optimization guarantees. In Fig. 4(a-b), we consider ten of the most difficult instances requiring more than a minute of computational time for Gurobi to find the best known solution. The one minute threshold is chosen as the problems that can be solved faster can be seen either intrinsically simple or their structure could be substantially simplified by the pre-processing techniques of Gurobi. The AIM solver is up to three orders of magnitude faster in all QUMO except the two instances, one of which it is unable to solve. Moreover, the AIM solver finds the new best solutions for two heavily constrained instances in about 40 seconds: the instances 3584 and 3860 have about 500 binary and 10000 continuous variables in QUMO formulation. To evaluate the speed-up, we run Gurobi for these two instances for five days. For the instance 3584, Gurobi finds the same solution as the AIM solver in about 54000 seconds, while proving its global optimality takes four and half days. The Gurobi solver optimises instance 3860 to the same quality as the AIM approach in about 13000 seconds with an optimality gap of 8% in five days.

Figure 4: Simulated AIM solver performance. (a) The relative speed-up performance of the AIM solver compared to the Gurobi solver is shown on QUMO instances formulated for a subset of QPLIB benchmark, namely instances with quadratic objective and linear inequality constraints for binary variables (QBL). The AIM solver is up to three orders of magnitude faster on eight out of ten instances, and is unable to solve one instance. For instances 3860 and 3584, the AIM solver finds the new state-of-the-art solutions. (b) The time performance is depicted for the Gurobi solver on the corresponding ten QBL instances in their original formulation. These are the hardest instances within the QBL instances that take more than 60 seconds for the Gurobi solver to find the best known solution. (c) The violin plots demonstrate distribution of the quality improvement performance for the AIM solver compared to the best solution found by competing methods across six QUBO benchmarks. The competing methods include parallel tempering, simulated annealing, and Gurobi solvers.



Although we do not know the origin of the hardest instances discussed above, we notice that the ones solved by the AIM approach are united by the same type of inequality constraints, which can be seen as Horn clauses [47]. The Horn clauses play fundamental role in automated theorem proving and, intuitively, imply that if all variables except one are true, then that last variable must also be true. Such insight into the logical properties of this subset of the hardest QPLIB problems may imply that the AIM solver can efficiently propagate the logical clauses of Horn type that can bring advantageous performance in solving logic programming problems.

In Fig. 4(c), the AIM solver demonstrates consistent objective improvement over the competing methods across several QUBO benchmarks including Wishart, RCDP, Tile3D, and QPLIB:QUBO, where QPLIB:QUBO includes a subset of graphs from QPLIB that are natively represented as the QUBO model. Remarkably, AIM solver finds new best solutions for the two largest problems with over thousand variables from QPLIB:QUBO, namely 3693 and 3850 instances. For Gurobi, the optimization of instance 3850 takes 110000 seconds to reach the same solution quality as AIM solver in 40 seconds, with the gap of 3% in 5 days. The instance 3693 cannot be optimised to the similar AIM quality of solution by Gurobi in 5 days. The AIM solver further demonstrates competitive performance on the G-Set instances. With many heuristic approaches applied to the G-Set benchmark over the past two decades, the performance of the Gurobi solver has probably been overlooked due to the general perception that it is inefficient at solving natively formulated QUBO problems. In our analysis, we observe that Gurobi solves particularly well instances with certain graph topologies, finding new best global solutions for four graphs with torus geometry from G-Set benchmark, although it still underperforms on other QUBO instances.

Among all QUBO benchmarks, AIM solver is behind only on the quadratic constrained binary optimization problems within QPLIB (QPLIB:QCBO), which includes instances with binary variables and equality constraints. We note that Gurobi employs various pre-processing techniques that can drastically reduce the number of variables and constraints [48], thereby greatly simplifying problems before invoking the main optimization methods such as simplex, interior point, and branch-and-bound.

With the development of similar pre-processing techniques for the AIM solver, the QUBO and QUMO formulations of constrained problems could be simplified and one could expect an improved performance for the AIM approach. For example,

we implement one of the pre-processing methods for solving two QUMO instances within QPLIB:QBL benchmark (see Methods).

Scalability Roadmap

The developed opto-electronic AIM architecture is the first tangible demonstration of a fully analog, spatially-multiplexed hardware that is able to solve optimization problems containing both binary and continuous variables with all-to-all connectivity. To address practical optimization problems at scale and guarantee the speed-up improvement, we envision the same proposed AIM architecture with 10000 variables using miniaturized and mass-produced opto-electronic components used, for example, in smartphone devices. For instance, the transaction settlement problem can be split into multiple sub-problems of that size based on transaction values and available liquidity. Another practical application at this scale could be the constrained portfolio optimization problem. For this problem, the whole universe of stocks, e.g. 2800 stocks within the New York Stock Exchange, can be represented within the 10000 variable hardware with all-to-all connectivity and mixed variables.

The AIM architecture with 10000 variables will be achieved by moving from discrete optical components to integrated opto-electronic technologies from the consumer space that are low-cost, low-power and scalable. Following the established operational principles of the AIM prototype, the most computationally expensive matrix-vector product will be still implemented in optical domain, while the annealing and momentum techniques will be realised in electrical domain. For generating and detecting optical signals, i.e., problem variables, one can use inexpensive and scalable micro-LEDs and CMOS sensors. To achieve sufficient system signal-to-noise ratios and dynamic ranges, each variable will be represented by multiple dependent optical sources detected by multiple dependent photodetectors. Spatial light modulators (SLMs) could be a promising technology for achieving high resolution modulator matrices, with potentially each individual SLM pixel representing a different problem weight. Estimating a source-to-SLM-pixel ratio of 1 : 100, micro-LEDs will shine onto rows of the modulators matrix to achieve the all-to-all connectivity. The modulated signals after the SLMs will be collected column-wise onto CMOS sensors to perform massive dot-product operations in parallel in a single pass of light through the system, as in [Fig. 1](#). These illuminations, elongated in one dimension, can be implemented

with spherical-lens systems, which are well-corrected for errors in large-field-of-view imaging [49].

Assuming that each SLM pixel can provide the required element-wise multiplication, an SLM resolution of 100 million pixels is needed to achieve a scale of tens of thousands variables. Since a typical SLM has several million pixels today, we envision the equivalent of a two-dimensional array of SLMs with a resolution of about 2000×2000 pixels each. We note that the current SLM refresh rate of a few hundred Hz is sufficient as the AIM solver needs to compute millions of samples for each optimization problem. Such an SLM, together with a 2000 array of independent micro-LEDs and a 2000 array of independent CMOS sensors, would constitute the key building block, i.e., single ‘module’ of the AIM solver. This module is then spatially multiplexed into an array of modules whose input and output signals are properly split and combined together guaranteeing a highly integrable platform for a large matrix by vector multiplication.

Keeping into account the industrial technological advancements of micro-LEDs and customized optical components, we calculate a total power consumption of the AIM hardware of about 2 kW at 10000 variables, including the contributions of transimpedance amplifiers and variable gain amplifiers. For the estimated 9 cm long overall path lengths of the whole hardware, we can achieve a time per iteration of approximately 0.6 ns.

On the digital side, we run the GPU-based solver implementation on A100 over a large number of synthetic instances with 10000 variables at FP16 precision. We measure the average time per iteration of 820 ns at the power consumption of 297 W. Assuming that the time per iteration will decrease by a factor of two as we move to INT8 to fairly compare the simulated results with the analog hardware, we calculate a speed up improvement of AIM versus state of the art digital hardware per unit power of about 100 times at 10000 variables. With such improvement, the same optimization problem would be solved in tens of seconds with the AIM hardware, while an hour long computation would be required for the digital solver.

Discussion

We face a pressing need for optimization hardware that can continue to scale in the edge computing era. The computational complexity of optimization problems forces us to rely on heuristics for finding approximate solutions. Heuristic algorithms running on a quantum computer with a million physical qubits would be still four orders of magnitude slower than alternative CPU-based algorithms [1]. To address the shortcomings of traditional classical and quantum hardware, we harness the speed of light and aim to build an opto-electronic computer to solve hard optimization problems at industrially-relevant scale more than two orders of magnitude faster than state-of-the-art digital solutions.

Reflecting on the practical impact of existing unconventional approaches in optimization, we focus on solving problems in the QUMO abstraction. The QUMO abstraction is superior to the well-known QUBO model, in which the objective variables are always binary, as it naturally expresses a broader class of optimization problems. The advantage of the QUMO abstraction is caused not only by the cost of converting continuous variables to binary, but also by the concomitant complexity increase for reformulated QUBO problems of larger size. On the contrary, QUMO can represent the ‘sweet spot’ between hardware amenability and higher expressive power for many practical applications. We observe that the heavily-constrained optimization problems, such as the transaction settlement or portfolio optimization problems, have a rather straightforward and efficient transformation to the QUMO abstraction.

To unleash the potential of analog computing, AIM provides an original view at unconventional optimization hardware. The AIM algorithmic approach not only shows highly-competitive performance across various benchmarks with four instances optimised to the new best ever solutions, but also offers advanced gradient-based approaches that are easily amenable for analog implementation. Following compute-in-memory principle, we utilize commodity technologies to build the first QUMO solver in analog hardware. The small-scale opto-electronic AIM based on discrete components solves the mixed binary and continuous optimization problems with weight matrices accuracy up to 7 bits in fully analog way. The good quantitative agreement between the simulated solver and its optical counterpart paves a promising

avenue for realising the state-of-the-art optimization approaches in analog hardware at scale.

We believe our blueprint for co-designing unconventional hardware and algorithms will ignite the exploration of other optimization techniques and hardware platforms, as well as enhance the development of automated problem mapping procedures to the QUMO abstraction. A wider variety of real world problems still need to be explored to understand which applications would benefit the most from the QUMO abstraction and for which the unconventional hardware, such as AIM, could bring a tangible advantage in terms of solution quality and time-to-solution for reasonably large problems. At scale of tens of thousands variables, AIM could provide a route to more cost-effective, energy-efficient, fast and accurate optimization architectures than conventional paradigms.

Methods

AIM Parameters

Typically, multiple hyperparameters need to be calibrated for heuristic methods to achieve their best performance in solving optimization problems. To determine the optimal set of parameters, external hyperparameter optimization packages or standard grid search techniques are widely used. While the choice of hyperparameters is critical, the time required to calibrate them is often overlooked. However, the hyperparameter space grows exponentially with the number of parameters, and a trade-off should be considered if the performance gain from fine-tuned additional parameters outweighs the time spent for fine-tuning them. In principle, the three main parameters $\{\alpha, \beta_0, \gamma\}$ of the AIM algorithm need to be adjusted for each optimization problem. In our simulations, we notice that the algorithm is less sensitive to momentum parameter value, while the α and β_0 values significantly affect the solution quality. We further perform a linear stability analysis of the AIM algorithm to evaluate reasonable exploration regions for these two parameters and find that by scaling the α parameter as $\alpha = \alpha_0/\lambda$, where λ is the largest eigenvalue of the weight matrix Q , we get scaled parameters α_0 and β_0 being in a similar optimal unit range across a wide range of problems.

We note that for two QPLIB:QUMO instances, namely 5935 and 5962, we developed a pre-processing technique that greedily picks variables with the highest impact on the objective functions and considers their possible values, which is accounted in the reported time speed-up of AIM.

The hardware performance is cross-validated with noisy simulations, in which the Gaussian noise is injected into variables with standard deviations of 3% for QUMO problems and 0.2% for QUBO problems to account for hardware imperfections. In addition, the measured hardware nonlinearity function is used for realising binary variables in the noisy simulations (further details are available in Suppl. materials). The smaller noise in case of QUBO model could be attributed to the fact that the weights of these instances are created to be sensitive to the noise in the first place. The momentum term is zeroed for noisy simulations. The relative and absolute tolerances are defined for some value a and its reference value a_{ref} as $|a - a_{ref}| \leq (\text{To}_{abs} + \text{To}_{rel}|a_{ref}|)$.

Comment on objective improvement metric. The introduced objective improvement metric can be used evaluate the relative improvement in objective value found by the solver of choice, i.e., the AIM algorithm, compared to other competing methods. In particular, the objective improvement of 100% happens when the AIM approach finds the best known objective while the competing solvers cannot achieve it, and in the reverse situation, the objective improvement is -100% when one of the competing solvers finds the best known objective while the AIM solver could not.

Competing solvers

For a fair comparison, we ensure that all methods use similar computing resources. Although the implementation of GPU or CPU based solvers can require highly varying engineering efforts, we try to estimate the cost of running solvers on the hardware, on which they are designed to run, and vary the time limit across solvers accordingly to ensure similar cost per solver run. In what follows, the AIM solver runs on GV100 GPU for 5 – 300 seconds per instance across all benchmarks. For the highest time limit of AIM we estimate time limits of about 400 seconds per instance for the simulated annealing and parallel tempering methods run on multicore CPU machine. In case of Gurobi, our licence allows one to use only up to 8 cores, so it is given 1000 seconds per instance. To simplify the evaluations, the competing solvers are always

given these maxed out time limits even for the instances on which AIM uses less than 300 seconds.

Simulated annealing. As described in Azure quantum inspired optimization service [31], simulated annealing is a Monte Carlo search type of method that simulates a state of varying temperatures, where the temperature of a state influences the decision-making probability. For optimization problems, the algorithm starts at an initial high-temperature state where “bad” moves in the system are accepted with a higher probability, and then slowly “cools” on each sweep until the state reaches the lowest specified temperature. At lower temperatures, moves that don’t improve the objective value are less likely to be accepted. For QUBO problems, each decision variable is “flipped” based on the objective value impact of that flip. Flips that improve the objective value are accepted automatically. Flips that don’t improve the objective value are accepted on a probabilistic basis, calculated via the Metropolis Criterion.

Parallel Tempering. As described in Azure quantum inspired optimization service [31], parallel tempering can be regarded as a variant of the simulated annealing algorithm, or more generally Monte Carlo Markov Chain methods [50]. As with simulated annealing, the cost function is explored through thermal jumps. Unlike simulated annealing, a cooling temperature is not used. Instead of running a single copy of the system, Parallel Tempering creates multiple copies of a system, called replicas, that are randomly initialized and run at different temperatures. Then the same process is followed as in simulated annealing, but based on a specific protocol two replicas can be exchanged between different temperatures. This change can enable walkers that were previously stuck in local optima to be bumped out of them, and thus encourages a wider exploration of the problem space.

Gurobi. Gurobi is the commercial solver that is highly-optimized to work as the black-box solver. Gurobi pre-solve techniques can drastically reduce the input problem size and the number of constraints [48]. We note that Gurobi finds for the first time the global minima solutions to several largest G-Set instances including G62, G72, G77, G81, which are all united by the same torus graph topology, and further proves that the best known solutions are exact for other graphs with torus topology: G11, G12, G13, G32, G33, G34, G48, G49, G50, G57, G65, G66, G67.

Benchmarks

QPLIB benchmark. The quadratic programming library (QPLIB) is a library of quadratic programming instances [30] collected over almost a year long open call from various communities, with the selected instances being challenging for state-of-the-art solvers. As described in the main part of the paper, we consider only the hardest instances within the QPLIB:QBL class of problems, which contains instances with quadratic objective and linear inequality constraints, the QPLIB:QCBO class of problems which contains instances with quadratic objective and linear equality constraints, and the QPLIB:QBN class of problems which contains QUBO instances.

Wishart benchmark. Wishart planted ensemble (WPE) problems [27] are originally planted binary Integer Linear Programming (ILP) problems whose coefficients are drawn from a correlated multivariate Gaussian distribution. It has been shown that in the hard regime, the ground state is extremely difficult to find using Monte-Carlo-based algorithms (such as parallel tempering) even for small problem sizes of 32 variables. The statistics has been collected across 100 instances

RCDP benchmark. Rotationally constrained discrepancy problem (RCDP) arises in the automotive manufacturing industry when one needs to arrange n disks on a common axis [51]. Due to imperfections, the disks have uneven surfaces and we wish to decide the alignment of disks to minimize total height. The disks have uneven surfaces due to imperfect machining. The goal is to rotate the disks to appropriate angles with respect to a reference orientation such that when all put through the common axel, the cumulative surface height in each sector is as close as possible to the ideal case when all surfaces are perfectly flat. This problem can be formulated as either mixed integer programming or QUBO. The RCDPs are tunable in hardness by increasing either n and the number of sectors K or the correlation between the sectors. For our study, the QUBO problems were generated by external team. The statistics has been collected across 100 instances with 360 variables.

Tile3D benchmark. The 3d tile planted problems [28] are highly tunable short-ranged Ising planted instances based on partitioning the problem graph into edge-disjoint subgraphs. It has been shown that the tile-planted problems can be made orders of magnitude (in terms of time-to-solution) harder than a typical 3D Gaussian spin-glass instance. The statistics has been collected across 100 instances with 512 variables.

G-Set benchmark. The G-Set benchmark includes a collection of synthetically generated instances from 800 to 20000 variables [52].

Hardware QUBO instances. For the hardware experiments, we generate 7-bit dense and sparse instances. The sparse instances belong to the QUBO model on three-regular graphs that is NP-hard [53], although NP-hardness does not imply that every random instance is difficult to solve. We apply two additional procedures to make these instances more challenging to solve. First, in order to ensure that the instances are not trivial to optimise, the global objective minimizer is verified to be distinct from the projected eigenvector corresponding to the largest eigenvalue of the weight matrix [54]. Second, the instances are made highly sensitive to noise as we generate a million instances and select ones that often lead to a different global objective solution in the presence of 1-bit level noise. For example, the generated instances with dense and sparse 7-bit weight matrices are likely to be affected by such small noise with a probability of 50 – 70%, which may translate to success rates of up to 30 – 50% for hardware that cannot guarantee the target 7-bit precision.

Hardware QUMO instances. Despite allowing several variables to have continuous values within the range of $[0, 1]$ in the QUBO instances above, these variables tend to retain their binary values. To ensure that the given variables take indeed continuous values in the global objective state, we plant random continuous minimizer values in the global solution and generate 10 QUMO instances with 7 variables. As the number of continuous variables increases for a given problem size, the problem instances become relatively easier to solve. Consequently, we consider instances with one, two, and three continuous variables.

References

- [1] R. Babbush et al. “Focus Beyond Quadratic Speedups for Error-Corrected Quantum Advantage”. *PRX Quantum* 2 (2021).
- [2] A. Marandi et al. “Network of time-multiplexed optical parametric oscillators as a coherent Ising machine”. *Nature Photonics* 8 (2014).
- [3] P. L. McMahon et al. “A fully programmable 100-spin coherent Ising machine with all-to-all connections”. *Science* 354.6312 (2016).
- [4] T. Inagaki et al. “A coherent Ising machine for 2000-node optimization problems”. *Science* 354.6312 (2016).

- [5] F. Cai et al. “Power-efficient combinatorial optimization using intrinsic noise in memristor Hopfield neural networks”. Nature Electronics (2020).
- [6] N. G. Berloff et al. “Realizing the classical XY Hamiltonian in polariton simulators”. Nature Materials 16.11 (2017).
- [7] K. P. Kalinin et al. “Polaritonic xy-ising machine”. Nanophotonics 9.13 (2020).
- [8] V. Pal et al. “Rapid fair sampling of the X Y spin Hamiltonian with a laser simulator”. Physical Review Research 2.3 (2020).
- [9] M. Babaeian et al. “A single shot coherent Ising machine based on a network of injection-locked multicore fiber lasers”. Nature Communications 10.1 (2019).
- [10] M. Parto et al. “Realizing spin Hamiltonians in nanoscale active photonic lattices”. Nature Materials 19.7 (2020).
- [11] D. Pierangeli, G. Marcucci, and C. Conti. “Large-scale photonic Ising machine by spatial light modulation”. Physical Review Letters 122.21 (2019).
- [12] C. Roques-Carnes et al. “Heuristic recurrent algorithms for photonic Ising machines”. Nature Communications 11.1 (2020).
- [13] S. AbdollahRamezani et al. “Analog computing using graphene-based met-alines”. Optics Letters 40.22 (2015).
- [14] N. V. Golovastikov et al. “Spatial optical integrator based on phase-shifted Bragg gratings”. Optics Communications 338 (2015).
- [15] S. Abdollahramezani et al. “Dielectric metasurfaces solve differential and integro-differential equations”. Optics Letters 42.7 (2017).
- [16] Y. Okawachi et al. “Demonstration of chip-based coupled degenerate optical parametric oscillators for realizing a nanophotonic spin-glass”. Nature communications 11.1 (2020).
- [17] J. J. Hopfield. “Neural networks and physical systems with emergent collective computational abilities.” Proceedings of the National Academy of Sciences 79.8 (1982).
- [18] J. J. Hopfield and D. W. Tank. ““Neural” computation of decisions in optimization problems”. Biological Cybernetics 52.3 (1985).
- [19] B. Jacobs. Quantum-Inspired Classical Computing (QuICC). HR001121S0041. Call for Proposals. report. DARPA - Microsystems Technology Office, 2021.
- [20] D-Wave machine. 2023. URL: <https://www.dwavesys.com/>.

- [21] L. Braine et al. “Quantum algorithms for mixed binary optimization applied to transaction settlement”. IEEE Transactions on Quantum Engineering 2 (2021).
- [22] J. E. Beasley. “Portfolio Optimisation: Models and Solution Approaches”. Theory Driven by Influential Applications. INFORMS, 2013. Chap. 11.
- [23] T. Böhlke, U.-U. Haus, and V. Schulze. “Crystallographic texture approximation by quadratic programming”. Acta Materialia 54.5 (2006).
- [24] D. L. Donoho. “Compressed sensing”. IEEE Transactions on Information Theory 52.4 (2006).
- [25] L. Braine et al. “Quantum Algorithms for Mixed Binary Optimization Applied to Transaction Settlement”. IEEE Transactions on Quantum Engineering 2 (2021).
- [26] G-set instances. URL: <https://web.stanford.edu/~yyye/yyye/Gset/>.
- [27] F. Hamze et al. “Wishart planted ensemble: A tunably rugged pairwise Ising model with a first-order phase transition”. Physical Review E 101.5 (2020).
- [28] F. Hamze et al. “From near to eternity: spin-glass planting, tiling puzzles, and constraint-satisfaction problems”. Physical Review E 97.4 (2018).
- [29] F. Hamze. “Rotationally-Constrained Discrepancy Problems (RCDPs)”. Unpublished (2022).
- [30] F. Furini et al. “QPLIB: a library of quadratic programming instances”. Mathematical Programming Computation 11 (2 2019).
- [31] Microsoft Quantum Inspired Optimisation (QIO) provider. 2022. URL: <https://learn.microsoft.com/en-us/azure/quantum/provider-microsoft-qio>.
- [32] Gurobi optimizer reference manual. 2023. URL: <http://www.gurobi.com>.
- [33] E. Valiante et al. “Computational overhead of locality reduction in binary optimization problems”. Computer Physics Communications 269 (2021).
- [34] B. T. Polyak. “Some methods of speeding up the convergence of iteration methods”. Trans. from the Russian by H. P. Cleaves. USSR Computational Mathematics and Mathematics (1962).
- [35] N. Qian. “On the momentum term in gradient descent learning algorithms”. Neural Networks 12.1 (1999).

- [36] S. Reifenstein et al. “Coherent ising machines with optical error correction circuits”. Advanced Quantum Technologies 4.11 (2021).
- [37] J. W. Goodman, A. Dias, and L. Woody. “Fully parallel, high-speed incoherent optical method for performing discrete Fourier transforms”. Optics Letters 2.1 (1978).
- [38] T. Wang et al. “An optical neural network using less than 1 photon per multiplication”. Nature Communications 13.1 (2022).
- [39] S. Kirkpatrick and D. Sherrington. “Solvable model of a spin-glass”. Phys. Rev. Lett 35.26 (1975).
- [40] S. Gedin. Securities settlement optimization using an optimization software solution. 2020.
- [41] F. Furini and E. Traversi. QPLIB: A Library of Quadratic Programming Instances. Zuse Institute Berlin. 2021. URL: <http://qplib.zib.de/> (visited on 01/20/2023).
- [42] D. Perera et al. “Chook—A comprehensive suite for generating binary optimization problems with planted solutions”. arXiv preprint arXiv:2005.14344 (2020).
- [43] Interactive charts comparing the results of Hans Mittelmann’s benchmarks. 2023. URL: <https://mattmilten.github.io/mittelmann-plots/>.
- [44] M. Aramon et al. “Physics-inspired optimization for quadratic unconstrained problems using a digital annealer”. Frontiers in Physics 7 (2019).
- [45] M. Mohseni et al. “Nonequilibrium Monte Carlo for unfreezing variables in hard combinatorial optimization”. arXiv preprint arXiv:2111.13628 (2021).
- [46] B. Tasseff et al. “On the Emerging Potential of Quantum Annealing Hardware for Combinatorial Optimization”. arXiv preprint arXiv:2210.04291 (2022).
- [47] J. N. Hooker and M. A. Osorio. “Mixed logical-linear programming”. Discrete Applied Mathematics 96 (1999).
- [48] T. Achterberg et al. “Presolve reductions in mixed integer programming”. INFORMS Journal on Computing 32.2 (2020).
- [49] T. Wang et al. “An optical neural network using less than 1 photon per multiplication”. Nature Communications 13.1 (2022).
- [50] E. Marinari and G. Parisi. “Simulated tempering: a new Monte Carlo scheme”. Europhysics letters 19.6 (1992).

- [51] F. Hamze. “Rotationally-Constrained Discrepancy Problems (RCDPs)” (2023).
- [52] C. Helmberg and F. Rendl. A Spectral Bundle Method for Semidefinite Programming. report SC 97-37. Konrad-Zuse-Zentrum für Informationstechnik Berlin, 1997.
- [53] M. R. Garey, D. S. Johnson, and L. Stockmeyer. “Some simplified NP-complete problems”. Proceedings of the sixth annual ACM Symposium on Theory of Computing. 1974.
- [54] K. P. Kalinin and N. G. Berloff. “Computational complexity continuum within Ising formulation of NP problems”. Communications Physics 5.1 (2022).
- [55] R. Brown et al. “Coptitive programming for mixed-binary quadratic optimization via Ising solvers”. arXiv preprint arXiv:2207.13630 (2022).
- [56] M. P. Harrigan et al. “Quantum approximate optimization of non-planar graph problems on a planar superconducting processor”. Nature Physics 17.3 (2021).
- [57] Y. R. Sanders et al. “Compilation of fault-tolerant quantum heuristics for combinatorial optimization”. PRX Quantum 1.2 (2020).
- [58] D. E. Rumelhart, G. E. Hinton, and R. J. Williams. “Learning representations by back-propagating errors”. Nature 323.6088 (1986).
- [59] A. Cordaro et al. “Solving integral equations in free space with inverse-designed ultrathin optical metagratings”. Nature Nanotechnology (2023).
- [60] R. Ashrafi et al. “Time-delay to intensity mapping based on a second-order optical integrator: application to optical arbitrary waveform generation”. Optics Express 23.12 (2015).
- [61] Z. Zhao et al. “Deep learning-enabled compact optical trigonometric operator with metasurface”. Photonix 3.1 (2022).
- [62] F. Zangeneh-Nejad and R. Fleury. “Performing mathematical operations using high-index acoustic metamaterials”. New Journal of Physics 20.7 (2018).
- [63] H. Goto, K. Tatsumura, and A. R. Dixon. “Combinatorial optimization by simulating adiabatic bifurcations in nonlinear Hamiltonian systems”. Science Advances 5.4 (2019).
- [64] H. Goto et al. “High-performance combinatorial optimization based on classical mechanics”. Science Advances 7.6 (2021).
- [65] M. Torii and M. T. Hagan. “Stability of steepest descent with momentum for quadratic functions”. IEEE Transactions on Neural Networks 13.3 (2002).

Author Contributions C.G., F.P. and H.B. conceived the project; K.P.K. and C.G. developed the abstraction with the support of N.G.B. and H.B.; K.P.K. and C.G. designed the algorithm with the support of N.G.B.; K.P.K. and C.G. ran the simulations and analyzed the simulations data; K.P.K. generated the QUMO and QUBO benchmarking used in the experiments; F.P., G.M.-A., and I.H. designed the experiment; G.M.-A performed the experiments; G.M.-A and K.P.K. analyzed the experimental data; D.C. contributed technical advice and support on the electronic circuit design and implementation; V.L. developed the automatized software for all the devices and equipments used in the experiments; L.P. and J.C. contributed technical advice and ideas; K.P.K., F.P., G.M.-A, C.G and H.B. wrote the manuscript; A.R. supervised the project. K.P.K. and G.M.-A. are the main contributors to this work and are listed in order of contributions. The rest of the authors are listed alphabetically by last name.

Acknowledgments The authors wish to thank Lee Braine, Barclays chief technology office, for useful discussions about optimization problems and QUMO abstraction; Stephen Jordan, Brad Lackey, Amin Barzegar, Firas Hamze, Matthias Troyer and the MS Quantum team for useful discussions about optimization problems and for providing us with the QUBO benchmarks (Wishart, Tile3D, RCDP). We acknowledge helpful discussions, encouragement, and support from our colleagues at Cloud Systems Futures at Microsoft Research, Cambridge, UK, and at M365 Research, Microsoft, Redmond, USA. N.G.B. thanks the Julian Schwinger Foundation grant JSF-19-02-0005 for the financial support.

Competing Interests The authors of the paper have filed several patents relating to subject matter contained in this paper in the name of Microsoft Co.

Correspondence Correspondence and requests for materials should be addressed to project-aim-contact@microsoft.com.

Supplementary Information

1 Problem mapping advantage of QUMO abstraction over QUBO model

The realistic optimization problems are commonly constrained problems with mixed variable types. The advantage of transforming an optimization problem to QUMO abstraction rather than QUBO model is evident for a wide class of problems including such with both binary and continuous variables, and problems with inequality constraints. To illustrate this mapping advantage, we consider a toy quadratic optimization problem with a linear constraint formulated in Fig. 1:

$$\text{Original problem : } \min ax_1x_2 + bx_3 \quad (4)$$

$$s.t. \quad 0 \leq cx_1 + dx_3 \leq 1, \quad (5)$$

in which all three variables can be assumed to be binary $x_i \in \{0, 1\}$. To get an unconstrained optimization problem, the inequality constraint can be mapped to the objective by using a penalty method:

$$\text{Unconstrained problem : } \min ax_1x_2 + bx_3 + P_0(cx_1 + dx_3 + s - 1)^2, \quad (6)$$

where $s \in [0, 1]$ is the continuous slack variable and P_0 is a large enough constant that ensures that the constraint is satisfied. A QUMO solver can be applied directly to this unconstrained optimization problem. In contrast, if one has a QUBO solver, then the additional mapping step needs to take place. To map a continuous variable to binary representation, one may consider either unary or binary encodings:

$$\text{Unary encoding : } s = \sum_{j=1}^{2^{N_{bits}}} y_j \quad (7)$$

$$\text{Binary encoding : } s = \sum_{k=0}^{N_{bits}-1} 2^k y_k, \quad (8)$$

where N_{bits} is the target bit precision for the continuous variable. From this simple analysis, the problem mapping to the QUMO abstraction is one-two orders of magnitude more efficient than to QUBO model in terms of the total number of variables. For the hardware QUBO solvers, the available bit precision for the input problem weights needs to be taken into account, which may limit one to use unary encoding.

2 Comment on QUMO abstraction

The introduced QUMO abstraction can be seen as a subclass of mixed integer non-linear programming (MINLP) class of problems. The MINLP problems appear in various fields including engineering design problems, particularly in chemical engineering where complex chemical processes can be modelled using quadratic or other nonlinear functions, and integer variables can represent discrete decisions. These optimization problems have a wide range of applications in areas such as chemical process design and control, network design, planning and scheduling, energy systems, and portfolio optimization. To address these problems, a variety of tailored algorithms have been developed that outperform general-purpose MINLP solvers. Given the increasing number of applications for MINLP and the growing demand for powerful analytics and decision-making tools, significant algorithmic developments are likely to emerge in this area over the next decade, including advances in convexification, decomposition, and parallel implementations to handle large-scale problems arising in machine learning.

Within MINLP, the mixed binary quadratic programming (MBQP) class [55] would include constrained optimization problems with binary and continuous variables, which is often also referred to as mixed binary optimization (MBO) problems [25]. Recent advancements in quantum and quantum-inspired technologies, as well as in optical Ising solvers capable of approximately searching for the ground state of Ising spin Hamiltonians, have increased interest in integrating Ising problems into the process of solving difficult optimization problems. Existing approaches range from direct mapping of MBQP to hybrid quantum-classical methods based on optimization algorithms [55, 25]. The problems within MBQP class with linear constraints could be efficiently translated to the QUMO abstraction with an additional continuous variable per each inequality constraint, making a wide range of applications more accessible for solving directly on AIM.

3 Quantum hardware limitations for optimization problems

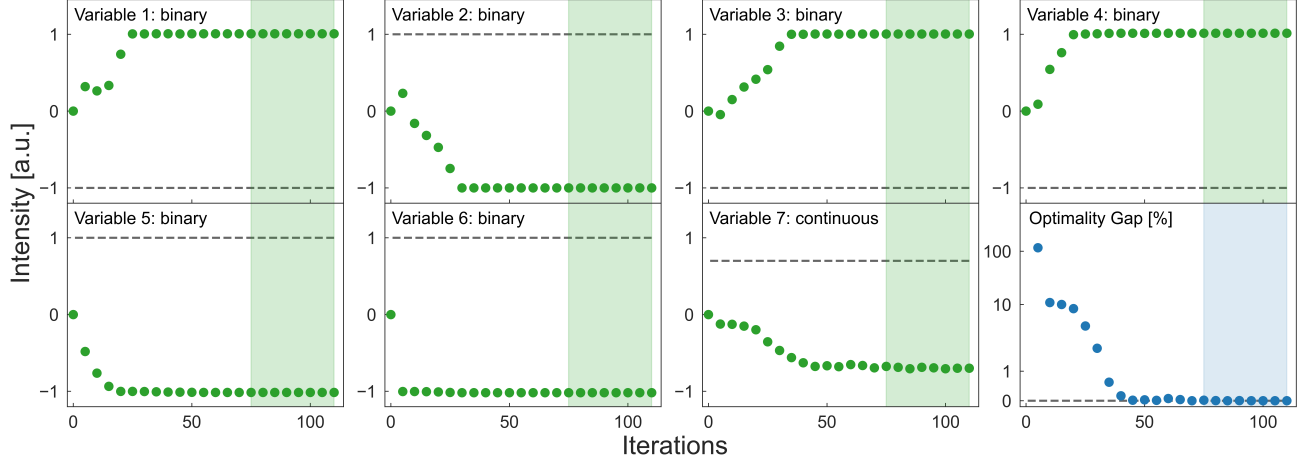
Quantum computing has emerged as a candidate hardware solver for hard optimization problems [56]. Similar to the other physical machines, quantum computers also

target the QUBO abstraction. In addition to sharing the same abstraction limitations, additional quantum hardware constraints further limit the potential of quantum computing as efficient solver for optimization problems. Quantum approximate optimization algorithm (QAOA), that targets quantum gate computers, performs similar to random guess on small-size QUBO problems [56] with theoretical estimations that even a million physical qubit hardware will be still many orders of magnitude slower than existing classical heuristics [57]. The quantum computers can offer up to quadratic speed-up over classical alternatives in solving NP-hard optimisation problems, to which QUBO and QUMO belong. But, this quadratic speed-up further suffers from the slow time operation of quantum gates. Hence, unless new quantum optimization algorithms emerge and quantum computers scale significantly, it is unlikely that quantum computing will allow us to tackle challenging optimization problems at sizes of interest.

Quantum annealing platforms offer another approach for solving QUBO problems. The D-Wave pioneered QUBO hardware solvers and managed to scale from tens of variables to the current several thousands of variables over two decades [20]. In practice, one of the main challenges for this hardware is the limited connectivity of only 15 connections per each variable, i.e. the Pegasus topology. This translates to additional mapping overhead of QUBO problem with an arbitrary topology to the D-Wave machine. In the worst case of the fully-connected graph, the latest D-Wave Advantage hardware with 5000 qubits can accommodate only problem sizes up to 150 variables. This one order of magnitude mapping overhead is further amplified by one-two orders of magnitude mapping advantage of QUMO over QUBO abstraction.

4 Examples of hardware time traces for QUMO problems.

The time evolution of variables and optimality gap are shown for QUMO problems with one and two continuous variables in [Supp. Fig. 1](#) and [Supp. Fig. 2](#), respectively. Initially, the feedback loop is open in opto-electronic setup and all variables are set to zero. Once the feedback loop is closed, the iterative update rule of the AIM algorithm happens for about 100 iterations and the variables, i.e. signal intensities, evolve to their steady states. The final steady state has near 0% optimality gap and corresponds to the global minimum objective, as verified with the Gurobi solver.



Extended Data Figure 1: Hardware time traces for QUMO problem with 1 continuous variable. The signal intensities (green) and the corresponding objective optimality gap (blue) are shown as a function of time iterations for the 7-bit QUMO problem with 6 binary and 1 continuous variables. The filled light green and blue areas represent regions for steady state detection. The expected variable values and zero optimality gap are shown with grey dashed lines. For the optimality gap graph, the symlog scale is used for y-axis for gap value over 1 and linear scale for values below.

5 Physical analogy of the AIM algorithm

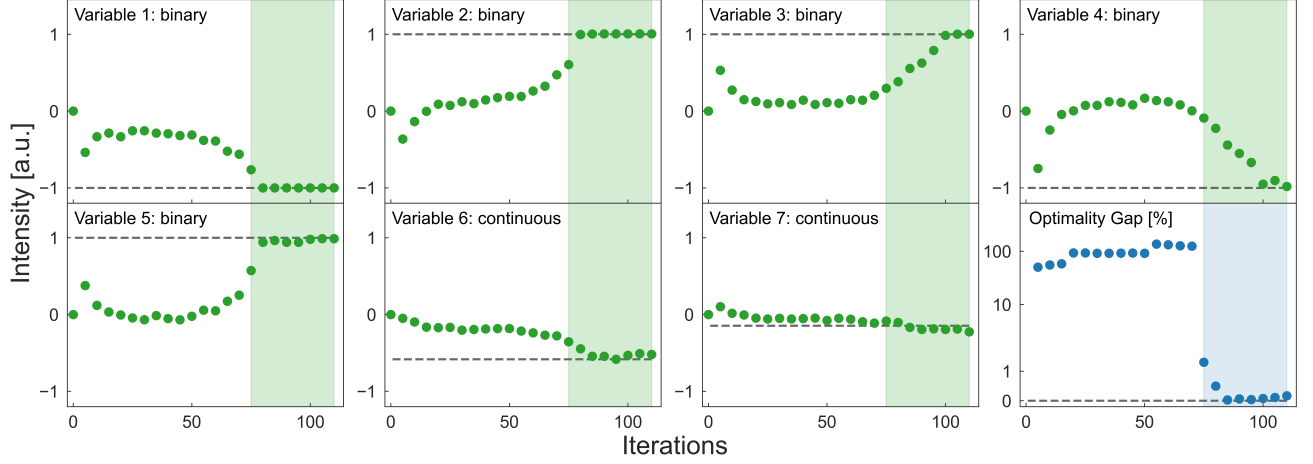
AIM algorithm belongs to the family of gradient descent methods that use the concept of momentum. The first momentum method has been introduced in 1964 by Boris Polyak [34] and is known as heavy-ball method or simply momentum method. For optimising the nonlinear function $F(x)$, it could be written as:

$$\mathbf{x}_{t+1} = \mathbf{x}_t + \Delta t [-\alpha \nabla F(\mathbf{x}_t) + \gamma(\mathbf{x}_t - \mathbf{x}_{t-1})], \quad (9)$$

As discussed in the main text of the paper, the AIM algorithm is the advanced gradient descent method represented by the iterative update rule:

$$\mathbf{x}_{t+1} = \mathbf{x}_t + \Delta t [-\alpha \nabla F(\mathbf{x}_t) - \beta(t)\mathbf{x}_t + \gamma(\mathbf{x}_t - \mathbf{x}_{t-1})]. \quad (10)$$

The momentum γ -term helps to overcome the issue of slow convergence due to fluctuations from one iteration to the next, which can cause the state to ‘bounce’



Extended Data Figure 2: Hardware time traces for QUMO problem with 2 continuous variable. The signal intensities (green) and the corresponding objective optimality gap (blue) are shown as a function of time iterations for the 7-bit QUMO problem with 5 binary and 2 continuous variables. The rest of description of [Supp. Fig. 1](#) applies here as well.

around an optimum instead of continuously moving towards it. The momentum term reduces the ‘bouncing’ by pushing consequent updates in the direction of the most recent update [58]. This effect provides a tendency for a system to continue along the path it is already taking, therefore making it less susceptible to ‘bouncing’ due to fluctuations in the gradient. For example, if a variable equals to 1 at iteration i and is -1 on the iteration $i + 1$, then this variable will be pushed at the iteration $i + 2$ by the momentum term for a value of 2γ , which provides a good local minima escape mechanism for the AIM algorithm. The parameter γ is generally less than 1 as the dependence of a given state on previous states should weaken with the number of iterations between the current state and the earlier state.

The physical interpretation for the momentum method [Equation 9](#) is well-known: in terms of continuous dynamical system, the momentum parameter is equivalent to the point mass m of Newtonian particles moving in viscous medium with friction coefficient μ under conservative force field $f = \nabla E$ with potential energy $E(x)$ [35]:

$$m \frac{d^2 \mathbf{x}}{dt^2} + \mu \frac{d\mathbf{x}}{dt} = -\nabla E(\mathbf{x}_t). \quad (11)$$

Similarly, the iterative update rule in [Equation 10](#) could be interpreted as the dynamical system of equations:

$$m \frac{d^2 \mathbf{x}}{dt^2} + \mu \frac{d\mathbf{x}}{dt} = -\nabla F(\mathbf{x}) - \phi(t)\mathbf{x}, \quad (12)$$

where $\phi(t)$ is the nonconservative force. To find the relation between physical quantities and parameters α , β , and γ , one can discretise the [Equation 12](#):

$$m \frac{\mathbf{x}_{t+\Delta t} - 2\mathbf{x}_t + \mathbf{x}_{t-\Delta t}}{\Delta t^2} + \mu \frac{\mathbf{x}_{t+\Delta t} - \mathbf{x}_t}{\Delta t} = -\nabla F(\mathbf{x}_t) - \phi(t)\mathbf{x}_t, \quad (13)$$

which can be further rewritten as

$$\mathbf{x}_{t+\Delta t} = \mathbf{x}_t - \frac{\Delta t^2}{m + \mu\Delta t} \nabla F(\mathbf{x}_t) - \frac{\Delta t^2}{m + \mu\Delta t} \phi(t)\mathbf{x}_t + \frac{m}{m + \mu\Delta t} (\mathbf{x}_t - \mathbf{x}_{t-\Delta t}). \quad (14)$$

By comparing terms in [Equation 10](#) and [Equation 14](#), we get:

$$\alpha\Delta t = \frac{\Delta t^2}{m + \mu\Delta t} \quad (15)$$

$$\beta(t)\Delta t = \frac{\Delta t^2}{m + \mu\Delta t} \phi(t) \quad (16)$$

$$\gamma\Delta t = \frac{m}{m + \mu\Delta t}. \quad (17)$$

Thus, the Newtonian system of equations, described by [Equation 12](#), is equivalent to the AIM iterative update rule, described by [Equation 10](#), with the parameters α representing the scaling factor of the conservative force, $\beta(t)$ standing for the nonconservative force, and γ corresponding to the particle mass.

The AIM algorithm converges to steady states for any positive values α , $\beta(t)$, and γ . These steady states are the minima of the Lyapunov function, representing the energy of the system. Denoting $y = f_{\text{nonlinear}}(x)$ to represent either binary or continuous variables, achieved by applying the elementwise nonlinear function for binary variables and linear function for continuous variables, the Lyapunov function can be written for the QUMO objective $F(y)$ for [Equation 12](#) as:

$$E = \frac{m}{2} \frac{df_{\text{nonlinear}}^{-1}(\mathbf{y}^T)}{dt} \frac{df_{\text{nonlinear}}^{-1}(\mathbf{y})}{dt} - \frac{1}{2} \mathbf{y}^T Q \mathbf{y} - b^T \mathbf{y} + \phi(t) \sum_{i=1}^N \int_0^{y_i} f_{\text{nonlinear}}^{-1}(x) dx. \quad (18)$$

Due to presence of nonconservative force, the overall improving QUMO objective value during the time evolution can be worsening for several intermediate consecutive

iterations. Towards the end of the time evolution, the annealing term $\phi(t)$ decreases to zero and the kinetic term vanishes, so the minima of the Lyapunov function correspond to the equilibrium states of the [Equation 12](#) and are the minima of the [QUMO](#) objective function. From the physics perspective, the convergence to the overall better optimal state in the end happens as the energy decreases due to the presence of friction.

We note that the promising results of analog computations have been demonstrated for solving differential equations and performing complex mathematical operations. For example, the Fredholm integral equations of the second kind can be solved using free-space visible radiation [\[59\]](#), the Hilbert transformation can be performed with a second-order optical integrator [\[60\]](#), the basic trigonometric operations are enabled with metasurface-based platform [\[61\]](#), and mathematical operations can be performed using high-index acoustic metamaterials [\[62\]](#).

6 Comparison of the [AIM](#) architecture to other iterative approaches

In case of the [QUMO](#) objective function, the simulated iterative update rule of the [AIM](#) algorithm reads as:

$$\mathbf{x}_{t+1} = \mathbf{x}_t + \Delta t [\alpha(Qf_{\text{nonlinear}}(\mathbf{x}_t) + b^T) - \beta(t)\mathbf{x}_t + \gamma(\mathbf{x}_t - \mathbf{x}_{t-1})], \quad (19)$$

$$f_{\text{nonlinear}}([\mathbf{x}_t]_i) = \begin{cases} \text{sign}([\mathbf{x}_t]_i), & \text{if } [\mathbf{x}_t]_i - \text{binary} \\ [\mathbf{x}_t]_i, & \text{if } [\mathbf{x}_t]_i - \text{continuous,} \end{cases}$$

where each variable $[\mathbf{x}_t]_i$ is also clipped to the range of $[-1, 1]$. For the well-studied [QUBO](#) model, the [AIM](#) algorithm can be further rewritten in a simpler form as:

$$\mathbf{x}_{t+1} = \mathbf{x}_t + \Delta t [\alpha(Q \cdot \text{sign}(\mathbf{x}_t) + b^T) - \beta(t)\mathbf{x}_t + \gamma(\mathbf{x}_t - \mathbf{x}_{t-1})]. \quad (20)$$

where all variables are now assumed to be binary. We choose sign nonlinearity here, but other nonlinearities could be considered including $\{\cos, \tanh, \text{clamp}\}$. As we discussed above in [section 5](#), the [AIM](#) iterative update rule corresponds to the second order differential equation. Consequently, the [AIM](#) algorithm is distinct from all the first order methods, the well-known example of which is the Hopfield networks [\[17\]](#),

18]. The Euler update rule and ordinary differential equation can be written for Hopfield networks as:

$$\mathbf{x}_{t+1} = \mathbf{x}_t + \Delta t [\alpha(Q \cdot \tanh(\mathbf{x}_t) + b^T) - \beta \mathbf{x}_t], \quad (21)$$

$$\frac{d\mathbf{x}}{dt} = \alpha(Q \cdot \tanh(\mathbf{x}) + b^T) - \beta \mathbf{x}. \quad (22)$$

In these equations, the losses term is represented by a constant parameter β . By considering time-varying losses $\beta(t)$ in Hopfield networks, one arrives to the equations, that are fundamentally similar to our current opto-electronic AIM implementation.

Another recently introduced heuristic method is called the simulated bifurcation algorithm [63, 64] which is described by equations:

$$\frac{d\mathbf{x}}{dt} = a_0 \mathbf{y}, \quad (23)$$

$$\frac{d\mathbf{y}}{dt} = c_0 Q \cdot \text{sign}(\mathbf{x}) - (a_0 - a(t))\mathbf{x}, \quad (24)$$

where a_0 , c_0 , and $a(t)$ are the hyperparameters. This system of equations can be further reduced to the single second order differential equation:

$$\frac{d^2 x}{dt^2} = c_0 Q \cdot \text{sign}(x) - (a_0 - a(t))x. \quad (25)$$

Compared to the AIM algorithm equations, the simulated bifurcation method doesn't have the first order derivative and its iterative update rule can be written as:

$$\mathbf{x}_{t+1} = \mathbf{x}_t + (\mathbf{x}_t - \mathbf{x}_{t-1}) + \Delta t^2 [-(a_0 - a(t))\mathbf{x}_t + c_0 Q \cdot \text{sign}(\mathbf{x}_t)]. \quad (26)$$

This update rule is similar to the AIM algorithm with $\gamma = 1$. In general, the momentum methods with $\gamma \geq 1$ are unstable [65]. Such instability is probably mitigated in the simulated bifurcation algorithm by an extra condition that manually forces the difference $(\mathbf{x}_t - \mathbf{x}_{t-1})$ to be zero if $|\mathbf{x}_t| = 1$. We also note that the original iterative update rule of the simulated bifurcation algorithm uses symplectic Euler method for discretising the system of equations above and can be written as:

$$\mathbf{x}_{t+1} = \mathbf{x}_t + a_0 \Delta t [(\mathbf{x}_t - \mathbf{x}_{t-1}) - \Delta t (a_0 - a(t))\mathbf{x}_t + \Delta t c_0 Q \cdot \text{sign}(\mathbf{x}_t)]. \quad (27)$$

which would suffer from the same instability issue due to the momentum term without applying the extra constraint above.

7 Extensions of AIM algorithm

Extension 1: other momentum-based approaches for the AIM algorithm. Momentum methods are commonly used in machine learning to accelerate the training of neural networks. Besides the heavy-ball method, one may modify the AIM algorithm to be based on, for example, the Nesterov momentum method, in which case the update rule would be given by the following equation:

$$\mathbf{x}_{t+1} = \mathbf{x}_t + \Delta t [-\alpha \nabla F(\mathbf{x}_t + \gamma(\mathbf{x}_t - \mathbf{x}_{t-1})) - \beta(t)\mathbf{x}_t + \gamma(\mathbf{x}_t - \mathbf{x}_{t-1})]. \quad (28)$$

Unlike heavy-ball method, the Nesterov momentum update evaluates the gradient at a point $(\mathbf{x}_t + \gamma(\mathbf{x}_t - \mathbf{x}_{t-1}))$, to which the momentum term has been applied, instead of evaluating the gradient at the most recent state \mathbf{x}_t .

The performance comparison between AIM algorithms based on different momentum-based methods is a promising avenue for future studies.

Extension 2: Exploration phase. In order to limit the range to be searched for each parameter, the initially defined bounds may be further dynamically updated based on a computed performance of solutions within the bound in comparison with solutions for parameters outside of the current bound. In other words, given a current bounds for $\alpha \in [\alpha_{min}, \alpha_{max}]$, by increasing the bound to, for example, $10 * \alpha_{max}$ and evaluating solutions for parameters within the increased bound, it may be determined that solutions outside the current bound are better than solutions inside the current bound and in this case the bound is increased. This process may be repeated over many iterations until a suitable region of parameter space is found.

8 Equivalence of QUBO, maximum cut, and Ising models

The QUBO, weighted maximum cut, and the problem of minimization of the classical Ising Hamiltonian are mathematically equivalent. The QUBO problem seeks to find assignments to a set of binary variables $x \in \{0, 1\}$ with the goal of minimizing the objective:

$$\min_x F_{\text{QUBO}} = \min_x -0.5\mathbf{x}^T A \mathbf{x} - \mathbf{a}^T \mathbf{x} - a_0 \quad (29)$$

where the matrix A , the vector a , and the constant a_0 are problem specific.

In the Ising model, one typically refers to variables as spins $y \in \{-1, 1\}$, to quadratic weights as interactions B , and to linear terms as magnetic fields \mathbf{b} . The objective is then to minimise the energy function:

$$\min_y F_{\text{Ising}} = -0.5\mathbf{y}^T B \mathbf{y} + \mathbf{b}^T \mathbf{y} + b_0. \quad (30)$$

Substituting $\mathbf{y} = 2\mathbf{x} - 1$ into [Equation 30](#), one gets the mapping between the QUBO and Ising models:

$$A = 4B \quad (31)$$

$$\mathbf{a} = 2\mathbf{b} - 2B\mathbf{e} \quad (32)$$

$$a_0 = b_0 - \mathbf{b}^T \mathbf{e} + 0.5\mathbf{e}^T B \mathbf{e} \quad (33)$$

where \mathbf{e} is the unity vector.

In the weighted maximum cut model, one looks for the cut of the given graph C into two parts with maximised number of their connecting weighted edges:

$$\max F_{\text{maxcut}} = \max_{E_1, E_2} \sum_{i \in E_1, j \in E_2} C_{ij} \quad (34)$$

where E_1 and E_2 represent vertices of two subgraphs. One can see the maximum cut model is equivalent to the problem of minimization of the Ising Hamiltonian by noticing that:

$$\max F_{\text{maxcut}} = \max_y \sum_{i,j} C_{ij} \frac{1 - y_i y_j}{2} = \max_y -0.5\mathbf{y}^T C \mathbf{y} + \sum_{i,j} C_{ij}. \quad (35)$$

We further note that the linear terms could be incorporated within quadratic terms by introducing an extra variable.